CFD analysis of a Darrieus Vertical-Axis Wind turbine installation on the rooftop of buildings under turbulent inflow conditions

Pradip Zamre[1] and Thorsten Lutz[1]

[1]University of Stuttgart, Institute of Aerodynamics and Gas Dynamics, Pfaffenwaldring 21, D-70569 Stuttgart, Germany

Correspondence: Pradip Zamre (zamre@iag.uni-stuttgart.de)

Abstract.

The behaviour of a rooftop mounted generic H-rotor Darrieus vertical axis wind turbine (H-VAWT) is investigated numerically in realistic urban terrain. The interaction of the atmospheric boundary layer with the different buildings, topography, and vegetation present in the urban environment leads to the highly turbulent inflow conditions with continuously changing inclination, and direction. Consequently, all these factors can influence the performance of a VAWT significantly. In order to simulate a small H-VAWT at rooftop locations in the urban terrain under turbulent inflow conditions, a computational approach is developed. First, the flow field in the terrain is initialized and computed with inflow turbulence. Later, the ~~wind turbine grids~~ **R1:AC1** mesh of wind turbine is superimposed on the mesh of the terrain at two distinct locations and different heights for further computation in the turbulent flow field. The behaviour of the H-VAWT is complex due to the 3D unsteady aerodynamics resulting from continuously changing the angle of attack, blade wake interaction, and dynamic stall. To get more insights into the behaviour of a rooftop mounted H-VAWT in turbulent flow, high fidelity DDES simulations are performed at different rooftop positions and compared the results against the behaviour at uniform inflow conditions in the absence of inflow turbulence, built environment. It is found that the performance of wind turbine is significantly increased near the rooftop positions. The skewed flow at the rooftop location increases the complexity. However, this effect contributes positively to increasing the performance of **R1:AC2** H-VAWT wind turbines.

1 Introduction

Wind energy is available in abundance, but it is not uniformly distributed. The growth of wind energy is **R1:AC3** mainly related to large-scale horizontal axis wind turbines (HAWTs), and wind farms located onshore and offshore. Though it is known for its potential, ~~the good offshore sites and unexploited windy areas are decreasing.~~ **R1:AC4** the available offshore sites are reducing because of expansions of wind farms. Considerable losses are associated with energy transportation from source to places where it is consumed **R1:AC5** (Gasch et al., 2012; Tosatto et al., 2021). Distributed and decentralized wind power is associated with the application of small, medium and, the lower end of large-scale wind turbine technologies (up to 2MW) in remote deployment or small-scale wind farms. Distributed and decentralized power generation emerges as complementary infrastructure to the conventional power systems that envisions electricity generation close to the consumption site e.g. urban/suburban environment, lowering the capital investments in transmission lines. The concept of urban wind energy is not new. In the past,

there have been already efforts to investigate the feasibility of harnessing the urban wind by installing small wind turbines on the roof of existing buildings or as stand-alone deployment in an urban area (Balduzzi et al., 2011; Mithraratne, 2009; van Wijk, 2011; Toja-Silva et al., 2013). Wind turbines can also be integrated with buildings, designed aerodynamically to accelerate the wind (KC et al., 2019; Karadag and Yuksek, 2020). It is a well-known fact that the mean wind speed in urban environments is lower than in open areas or rural areas. However, some locations tend to be windier such as rooftops, building edges, a passage between two buildings, etc. The interaction of the atmospheric boundary layer with the rough terrain and obstacle of different shapes and permeability present along the flow path leads to complex flow conditions in the built environment with lower velocities, high turbulence, and continuously changing direction. These conditions can severely influence the behaviour and dynamic loads of the small wind turbine.

1.1 Vertical axis wind turbines (VAWTs) in turbulent urban flow field

In general, the research areas of urban wind energy and small wind turbines overlap ~~with~~ each other. In the wind industry, wind turbines can be classified ~~based on their axis of rotation~~ in two categories, namely horizontal and vertical axis wind turbines **R1:AC6** based on their axis of rotation. The horizontal axis wind turbine concept has been proven mature, successful, and economical on a large scale, but it is wind direction-dependent. ~~Furthermore~~ **R1:AC7** Hence, it needs a yaw mechanism. In the built environment, the flow inclinations negatively affect the performance of a small HAWT (Bianchi et al., 2013). In this regard, the VAWT concept has several advantages in the urban environment. In skewed flow, the performance of the H-Darrieus VAWT rotor increases above the non-skewed flow (Mertens et al., 2003). It has the omni-direction **R1:AC8** wind catching capability. Thus no yaw mechanism is needed, which reduces mechanical complexity. VAWTs typically have fewer moving parts, and a generator can be installed at ground level. It could lead to lower maintenance costs and higher availability. The wake recovery of VAWT is faster than that of the HAWT **R1:AC9** **R2:Ma1** (Kinzel et al., 2012), which allows a dense cluster of wind turbines in the wind farm, increasing the power density **R1:AC9** (Dabiri, 2011). Also, the VAWT concept has potentially lower noise emissions than the HAWT of the same power class (Kern et al., 2019). However, the VAWT concept has some drawbacks. Its performance is lower than that of HAWT. The underlying physics behind the operation of VAWT is more complex than HAWT. The inherent unsteadiness is caused by the continuously changing angle of attack and relative velocity during the revolution.

The influence of turbulence on the behaviour of the VAWT is one of the significant research areas considering the applications of small VAWT in urban environments. One approach to investigate the influence of the turbulence on the VAWT is based upon correlating the performance and on-site wind measurements. Previously, Möllerström et al. (2016) studied a 200 kW Darrieus VAWT in an open field. Their study concluded that turbulence positively impacts energy extraction, and the effect is more evident at higher tip speed ratios. Also, the performance of the wind turbine and optimal tip speed ratio (λ) increase with turbulence intensity (TI) allowing optimization of control strategies to capture more high-energy wind gusts. Study of Berténi et al. (2012) also found that turbulence has no adverse effect on the performance of VAWT using "gust tracking". Pangini et al. (2015) compared the performance of a small commercial VAWT with HAWT of the same rated capacity of 20 kW installed at the Savona harbor. It is concluded that both wind turbines are sensitive to turbulence and not suitable for installation in

complex areas where turbulence levels are often high. Kooiman and Tullis (2010) studied the effects of wind velocity and direction fluctuations on the energy production of rooftop installed VAWTs in urban environments. The output power varied with wind velocity fluctuations but was roughly independent of the wind direction changes. Authors also compared data from urban environment testing with the earlier work of Bravo et al. (2006) on the same wind turbine in a low turbulence wind tunnel. It is found that the performance of wind turbine degraded marginally at TI < 15% compared to the smooth flow benchmark at TI < 2%. In all these discussed studies, there has been no consistency about the influence of the turbulence on the behaviour of VAWT. Also, replicating the flow characteristics from the urban environment in the wind tunnel poses serious challenges. Most of the wind tunnel facilities are designed for aerospace research with very low background turbulence intensity. ~~One may argue that the turbulence intensity and in an urban environment turbulence intensity can easily exceed 10%.~~ **R1:AC10** and in an urban environment large scales dominate the turbulence intensity, which can easily exceed 10%. The eddies size differs over a broader range of integral length scales. These factors limit the scope of addressing the topic of turbulence in the wind tunnel.

The advancement in computing capacities and infrastructure allow us to use of high-fidelity computational fluid dynamics (CFD) methods ~~extensively~~ to investigate complex flow behaviour. A broader range of approaches have been used to explore different aerodynamics phenomena of the VAWT. One of the earliest studies to model the influence of inflow turbulence on the VAWT was carried out by Brahimi and Paraschivoiu (1995). The effect of turbulence intensity on the performance of an offshore VAWT was investigated by Siddiqui et al. (2015) and found that performance deteriorates by almost 23% to 42% as turbulence intensity increases from 5% to 25%. Rezaeiha et al. (2018) studied the impact of different operational parameters on a H-Darrieus rotor along with turbulence intensity. Authors found that with an increase in turbulence level the dynamic stall at a low tip speed ratio is delayed and the power coefficient increases. However, at the optimal tip speed ratio, the turbulence has a relatively marginal influence. Also, the turbulence reduces the impact of the shaft wake on the blade forces in downwind passage. All these studies primarily focused on the influence of turbulence on the performance of the VAWT in controlled conditions but not in realistic conditions ordinarily present in the urban environment. Siddiqui et al. (2021) analyzed the effect of turbulence and ground clearance on the performance of a rooftop VAWT using three-dimensional RANS simulations. Contrary to study of Mertens et al. (2003), it was found that the performance of a VAWT enhanced at height, offering less ground shearing effect. Also, with increasing turbulence intensity, a drop in performance is observed. To the best of authors knowledge, there have been no high fidelity DDES or LES studies of a rooftop mounted H-Darrieus rotor available in realistic urban terrain and under turbulent inflow conditions.

1.2 Scope and objectives

This work aims to investigate the aerodynamic performance of a rooftop mounted H-Darrieus rotor vertical axis wind turbine in a realistic urban environment under turbulent inflow conditions considering the topography, different buildings, and large vegetation area. A large area is considered for the investigation to mimic the development of a realistic urban boundary layer. A generic reference H-Darrieus rotor is scaled up based on the geometrical parameter for the present work. As a basis for comparison, the scaled-up variant is analyzed at the uniform flow conditions. With the existing high-fidelity process

Figure 1. Aerial view of Morgenstelle campus (© Google Earth 2020) and Wind-rose from synthetic wind statistics (© 2021 Landesanstalt für Umwelt Baden-Württemberg).

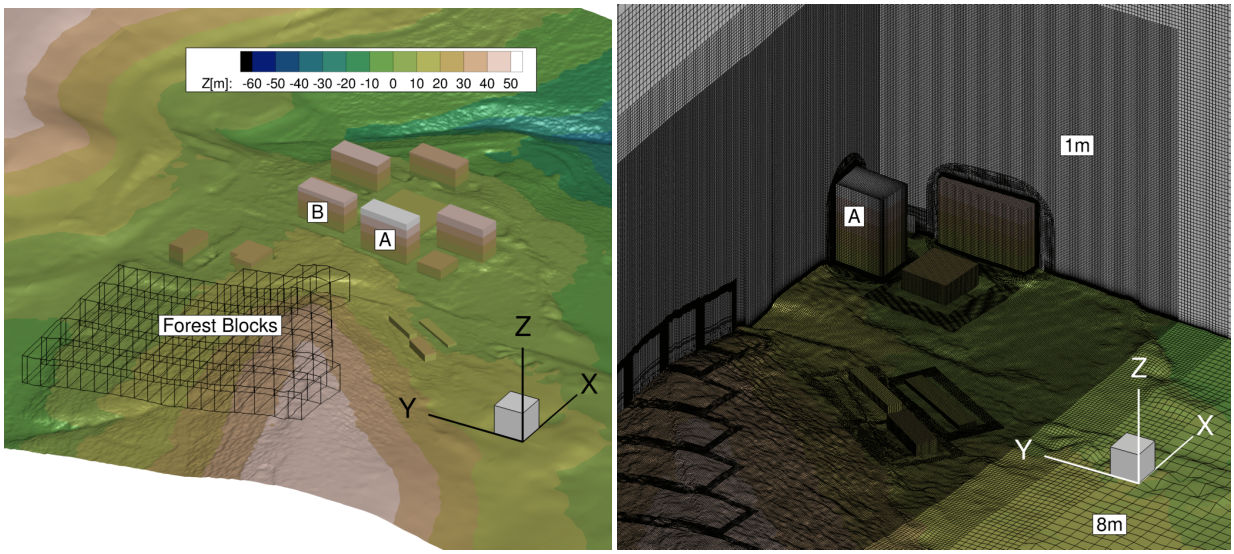

Figure 2. The urban terrain model and computational grid.

chain, the characteristic of H-Darrieus rotor can be analyzed at different heights over the rooftops buildings under resolved turbulent conditions. Variations in height are aimed at investigating wind turbine performance in different turbulence levels and inclinations. The power **R1:AC11** coefficients, normal and tangential loads are compared with the reference case at the uniform inflow.

2 Numerical Process chain

2.1 CFD solver

The FLOWer is a compressible, block-structured Reynolds Averaged Navier Stokes (RANS) solver developed by the German Aerospace Center (DLR) (Rossow et al., 2014). At the Institute of Aerodynamics and Gas Dynamics (IAG, University of Stuttgart), FLOWer is continuously ~~furthered~~ **R1:AC12** developed to incorporate new features and to improve its performance. The overlapping grid technique CHIMERA enables the assembly of independent grids of each component by embedding them into a background mesh (Benek et al., 2014). Furthermore, the solver is extended with the functionality of higher-order finite difference weighted essentially non-oscillatory (WENO) scheme (Schäferlein et al., 2014), and different Detached Eddy Simulation (DES) models (Weihing et al., 2018). Also, it has been extended with vegetation modeling capabilities (Letzgus et al., 2018). The FLOWer has proven capabilities for wind turbine and helicopter simulations in several projects.

2.2 Generation of inflow turbulence

The inflow turbulence is generated using the in-house code PROFGEN, which is adopted from the work of Mann (1992). This model is based on the von Karman iso-tropic spectrum $\phi(\kappa)$ and uses the rapid distortion theory to estimate the effect of shear. Three input parameters are required: length scale l_0, stretching factor Γ, and energy dissipation $\alpha\epsilon^{2/3}$. Here, l_0 and $\alpha\epsilon^{2/3}$ determine the magnitude and the distribution of energy in the spectral domain, respectively. Γ controls the level of shear and anisotropy.

The fluctuating components of atmospheric turbulence u' are transformed into a volume force term $\boldsymbol{f}_s$ and is applied to a transverse plane downstream from the inlet. It is defined as force per unit volume applied to accelerate the mean velocity field from $\bar{\boldsymbol{u}}$ to $\bar{\boldsymbol{u}} + \boldsymbol{u'}$, and as per Troldborg et al. (2014), is given by

$$\boldsymbol{f}_s = \frac{\rho \boldsymbol{u'}}{\Delta x}(\bar{u}_n + \frac{1}{2}u'_n) \tag{1}$$

Here $\bar{u}_n$ and u'_n, are the magnitude of the mean and the fluctuating velocity with index n, respectively. Δx is the grid spacing normal to the transverse plane.

2.3 Vegetation modeling

The forest blocks are modelled as a porous medium. The drag caused by the vegetation is added to the momentum and energy equations via the volume force source term. It is based on the approach of Shaw et al. (1992). The drag depends on the local foliage density $a(z)$. It is possible to model the forest heterogeneously, considering local foliage density and height values for different parts of the vegetated area. The drag source term is given by

$$F_w = -\rho c_d a(z)|u|\boldsymbol{u} \tag{2}$$

where, ρ, c_d, $|u|$ and $\boldsymbol{u}$ are density, the drag coefficient, local magnitude of velocity, and velocity vector, respectively. The Leaf Area Index (LAI) over the height is defined as

$$LAI = \int_{z}^{h} a(z)dz \tag{3}$$

A lower value of LAI represents sparse vegetation, while higher values of LAI represents dense vegetation.

2.4 Computational set-up

2.4.1 The H-Darrieus Turbine and its scaling

The examined wind turbine is based on a generic **R1:AC13** fixed pitched, two-bladed H-rotor VAWT designed by Li et al. (2016). It has a diameter of 2 m, a blade height of 1.2 m, a blade chord length of 0.265 m, fixed pitch of 6° and NACA0021 airfoil section. It has been investigated experimentally in the wind tunnel as well as in the field by Li et al. (2016). The blade cross-section area is constant over the complete blade length. The central shaft has a diameter of 0.216 m. For rooftop application in the present study, it is scaled up by a factor of 3.5, keeping the solidity constant. The solidity (σ) is calculated as follows

$$\sigma = \frac{nc}{D} \tag{4}$$

where n is the number of blades, c is the blade chord length, and D is the diameter of a VAWT, respectively.

Table 1. Scaling-up of VAWT.

Parameter	Original	Scaling Factor 3.5
Wind speed (ms^{-1})	8	8
Rotor diameter D (m)	2	7
Blade length L (m)	1.2	4.2
Blade chord c (m)	0.265	0.9275
Aspect ratio (L/D)	0.6	0.6
Turbine solidity (nc/D)	0.265	0.265

The scaled version has a rotor diameter of 7 m, a blade height of 4.2 m, a blade chord length of 0.9275 m, and a central shaft diameter of 0.756 m. Dimensions for the original and the scaled-up versions are given in Table 1. ~~The aspect ratio does not change after scaling.~~

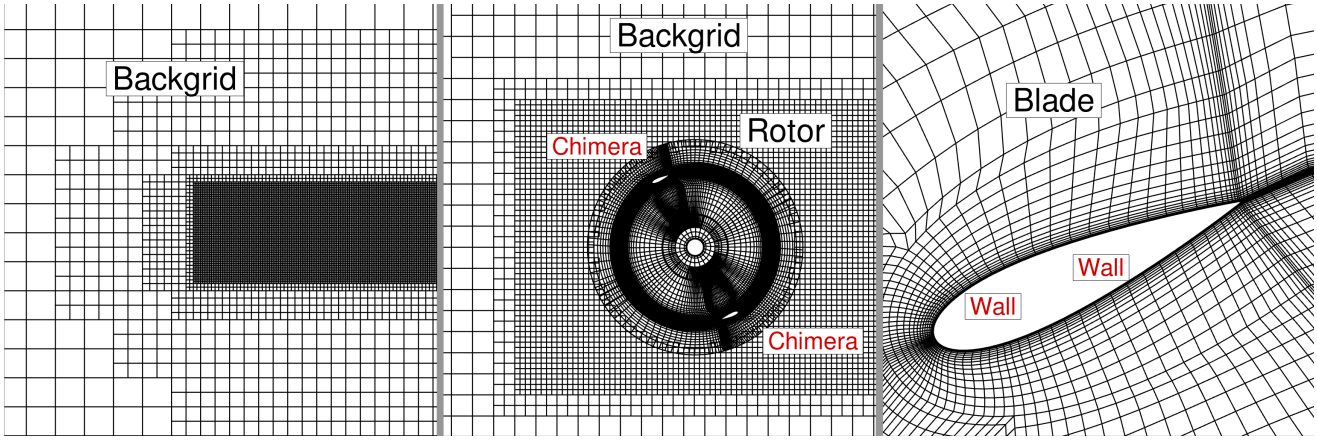

Figure 3. Computational grid of the H-VAWT for the uniform inflow study. Boundary conditions are shown in red colored text. (Not to the scale and every fourth cell of the mesh has been shown)

2.4.2 Terrain and wind direction

For the investigation, the "Morgenstelle" campus of the University of Tübingen from south Germany is selected, as depicted in Fig. 1. ~~Also,~~ **R1:AC14** The synthetic wind atlas data presented in Fig. 1 shows that the southwest is the main wind direction with densely forested hill lying in the upstream region of the built environment. There are 4-5 high-rise buildings with height of 40 m and more.

2.4.3 CFD model

R2:Ma2a The wind turbine at the original scale is numerically investigated and validated using the FLOWer flow solver at IAG by Dessoky et al. (2019). The results showed good agreement with experiments. In present study, computational set-up including time steps is consistent with Dessoky et al. (2019). As described in Sect. 2.4.1, the computation grids are also scaled with same scaling factor applied to the wind turbine. The blades and shaft grids have a fully resolved boundary layer ($y^+ \leqslant 1$) with 32 cell layers. ~~The shaft is considered only in the region of the rotor.~~ **R1:AC15** A shaft is considered in the simulation with a height being equal to the blade span. Blades are meshed using commercial mesh generation applications Pointwise and Gridgen. Based on the convergence study conducted for different grids of the original wind turbine using FLOWer, the selected blade mesh is composed of 336 cells in the chord-wise direction and 48 cells in the span-wise direction. The CHIMERA intersection area is defined near the outer periphery of the rotating zone to assemble the wind turbine in the background grid. No changes has been made in the wind turbine grid throughout the study.

The computational approach is discussed in the Sect. 2.5. For the investigations in uniform inflow, the background grid is created by using the in-house automated tool. The background grid is of Cartesian type and has dimension 215 m x 84.5 m x 76.8 m in x,y, and z-direction, respectively. The grid has hanging nodes enabling different levels of refinements. However, the background grid used for the uniform flow condition is not shown in this study. The near wake region has a grid refinement size

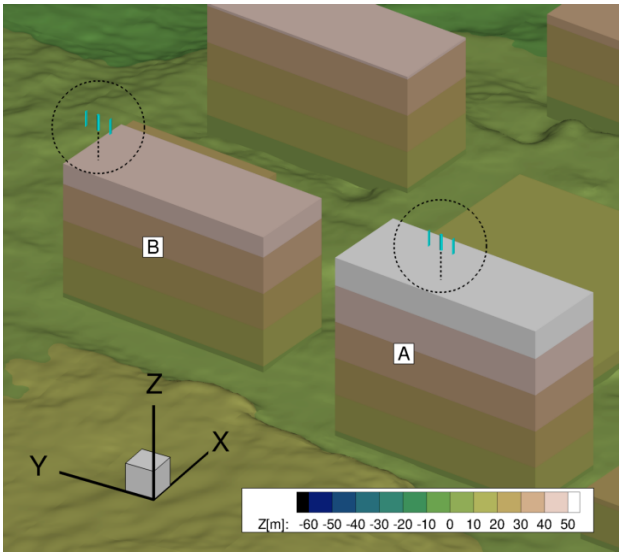

Figure 4. Rooftop mounted H-VAWTs **R1:AC16** ~~over~~ on top of buildings A and B.

of 8.625% of the chord shown in Fig. 3. No inflow turbulence is applied. The background grid specific to the uniform inflow investigations is not relevant to the urban terrain investigations.

In the case of urban terrain simulations, computation grids for the buildings are created using Pointwise and Gridgen. Different building structures, terrain, forested blocks, and the assembly of the computation grids are shown in Fig. 2. The Cartesian background grid of the terrain has the smallest cell size of 1 m in the region of interest, transiting to 8 m resolution in the remaining domain by the usage of hanging nodes. In order to resolve the inflow turbulence, a channel-like region from inlet to outlet is meshed with a resolution of 1 m, which covers all considered built environment along with the forest and topographical features. It results in 105 Million cells in the background mesh. The boundary layer for the terrain and buildings meshes, is resolved with 64 layers, which results in $y^+ \leqslant 2$. The extent of the background mesh is 1087 $\mathrm{m} \times 2432$ $\mathrm{m} \times 655$ m in x,y, and z-direction, respectively. The chosen values of LAIs for forest blocks vary from 1.8 to 2.0, corresponding to the winter season. For the **R1:AC17** overall investigation of the wind turbines in urban terrain, ~~overall,~~ a complete set-up consists of background mesh, two rotors, shafts, wake refinement regions and remaining built structures along with vegetation. Figure 4 shows the rooftop mounted H-VAWTs ~~over~~ **R1:AC18** on top of buildings A and B. It has approximately 153 million cells and 19000 blocks.

2.4.4 Boundary conditions and solver setup

In the case of ~~investigation in~~ uniform inflow with wind velocity 8 ms^{-1}, farfield boundary conditions are defined for all sides of the computational domain. ~~All the components of the turbine are treated as a no-slip walls.~~ **R1:AC19** No-slip boundary conditions has been introduced for the surfaces of all components..

For the investigation in the urban terrain, a generic log law profile based on ~~data from~~ the New European Wind Atlas is defined via a Dirichlet boundary condition at the inlet. At the start of the simulation, the whole computational domain is initialized with the wind profile. The lateral sides, topside, and outlet are realized as farfield boundary conditions with zero-order extrapolation. The ground and the surfaces of the rotors and the built environment are defined as no-slip walls. Turbulence intensity of 10% and a length scale of 50 m are used as input parameters to PROFEGN in order to generate inflow turbulence as per Kaimal spectrum. ~~It was~~ **R1:AC20** Turbulence is introduced by momentum source terms on the transverse plane at 96.5 m downstream from the inlet and approximately 450 m upstream from the built environment, which is under consideration.

For the present study, DDES simulations ~~were~~ **R1:AC21** are performed employing a dual time-stepping scheme for temporal discretization. Menter-SST model is used for turbulence modeling (Menter, 1994). A second-order scheme with the Jameson-Schmidt-Turkel (JST) artificial dissipation term (Jameson, 1981) is used for spatial discretization in the boundary layer. The fifth-order WENO scheme is applied to the background mesh to ensure less numerical dissipation and reconstruction of fluxes and more accurate propagation of vortical, turbulent structures.

2.5 Computational approach

R1:AC22 In the absence of the experimental or field measurements for the scaled-up VAWT, the performance at uniform inflow conditions without inflow turbulence is considered a basis for comparison with realistic conditions. However, experiential data is available for the original unscaled VAWT in Li et al. (2016). Ferreira et al. (2007) studied 2D VAWT numerically and experimentally. Authors showed that delayed eddy simulations (DES) reasonably predict the generation and shedding of vorticity. It also exhibits acceptable sensitivity to spatial and temporal grid refinement. It implies that scale resolving DES simulations can be used where validation data is limited or nonexistent. Therefore, the scaled-up VAWT is investigated by applying a high-fidelity approach at the reference condition of uniform inflow 8 ms^{-1} for different operating points in the first part of present study. The power coefficient vs. tip speed ratio **R1:AC23** $(C_P - \lambda)$ curve serves as ~~one of the~~ **R1:AC24** a basis for selecting the operating point and comparing the behaviour of the wind turbine in realistic urban terrain.

R1:AC25 The simulations of VAWT in urban terrain are divided in two sets with different purposes. In first set of simulations, VAWTs are not present. The injected turbulence is allowed to develop and propagate through the domain. Once the turbulent flow field is well-developed within the domain, the complete field solution is saved. As shown in the Fig.5, this field solution serves as starting point for the second set of simulations. After this instance, the earlier simulation is continued and the averaging of the flow variables is started in order to get mean wind profile, turbulence intensity and skew angles. As per recommended practices for the deployment of the wind turbines in the built environment (Fields et al., 2016), for the rotors more than 2 m diameter, ~~the heights for the reaching the acceptable wind speed and turbulence intensity should be the bottom of the rotor swept area.~~ **R1:AC26** the wind turbine should be positioned in such a way that it receives acceptable level of wind speeds and turbulence intensity. **R1:AC27** Based on the flow separation, mean wind speed and turbulence intensity, positions of wind turbines are chosen over the rooftop of each building A and B for second set of simulations. The details have been discussed in Sect. 3.2. At these two locations, three different heights 10 m , 12 m and 20 m are selected for VAWT

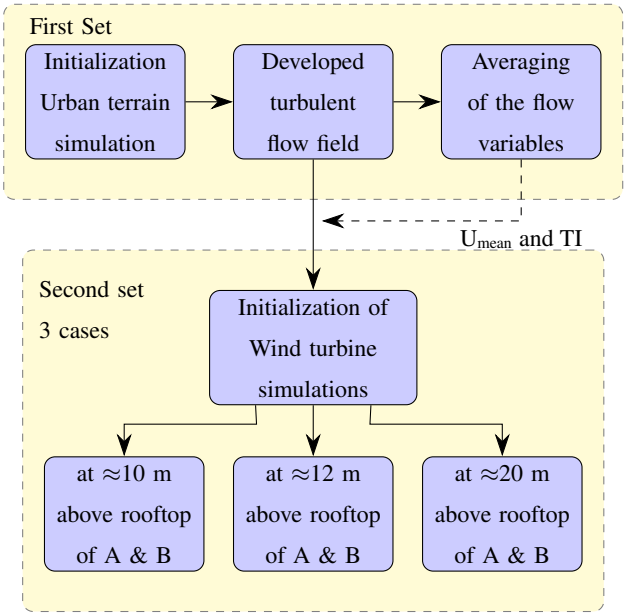

Figure 5. Computational approach for the investigation of VAWT in urban terrain under turbulent inflow conditions.

investigation. **R1:AC28** The rationale behind selecting the 20 m height is to compare the performance of the H-VAWT at relatively distant position from the rooftop with other two positions, which are near to rooftop. It is expected that the distant position from rooftop will be less influenced by the geometry of the buildings.

R1:AC29 From the saved field solution of the first set of simulation, second set of simulations are conducted. The meshes of wind turbines and wake refinement regions, are introduced to existing urban terrain solution and computational set-up at desired locations by interpolation as shown in Fig.5. The wind turbine meshes are initialized at reference flow velocity and simulated further for selected operating point. Similar procedure is repeated for remaining cases. **R1:AC30** With this approach, significant computation time is saved and it also increases pace of the simulation. Details have been discussed in Sect. 2.6. **R1:AC31** The urban terrain without wind turbines can be simulated with larger time step as there is no moving parts. However, in case of VAWT simulations the time step are smaller than terrain only simulation. Based on the mean wind speed at corresponding height and selected operating point, the rotational speed is calculated. It is kept constant throughout the simulations. ~~The~~ **R1:AC32** Active pitch control or dynamic changes in rotational speed depending on the fluctuations in the incoming wind are not considered. **R1:Ma3** **R1:AC61b** It is expected that the wind turbine will not run efficiently at selected tip speed ratio most of the time by keeping the rotational speed constant in the turbulent flow field. However, it is important to note that the fluctuations in the wind speed occur over very short time span. It would have been practically very difficult to adjust the tip speed ratio for every second/revolution during simulations. Therefore, for simplicity the tip speed ratio and rotational speed are assumed to be constant over the short time period considered in the evaluation of the turbine performance in turbulent inflow. A similar assumption can be found in studies of Li et al. (2016); Balduzzi et al. (2020);

Table 2. Overview of computational cost of different cases.

Simulation Cases	No. of cells (in Millions)	No. of cores	Time step [s]	Time required [Hrs]
Only urban terrain	127	8192	0.0278	69
Urban Terrain + 2 VAWTs (estimate)	153	8192	0.0031733	908
Urban Terrain + 2 VAWTs + current approach	127 (Set 1)/ 153 (Set 2)	8192	0.0278 (Set.1)/ 0.0031733 (Set 2)	330

Hohman et al. (2018) as well. Though, the turbulent inflow possesses higher energy content than uniform inflow, the energy is extracted at lower efficiency, as the consequence of optimal tip speed ratio is not maintained in turbulent inflow. Therefore, the moment and forces are averaged over 30 revolutions. This results in the maximum value of the power of the turbine at selected tip speed ratio and fixed rotational speed.

To sum up, ~~there are~~ three different parts with three different but interdependent objectives **R1:AC33** are included in the present study. In the first part, scaled-up VAWT is investigated at uniform flow conditions. In the second part, turbulent flow field in the urban terrain is analyzed, while in the third part, wind turbines are investigated in urban terrain under turbulent inflow conditions .

2.6 Computation Time

R1:Ma1 **R1:AC78** As discussed in Sect. 2.5, there are three parts in the present study. Out of these three parts, it is obvious that due to terrain second and third part need significant computation time. Table 2 provides information about computation time needed for different approaches. The second part focuses on only terrain simulations under turbulent inflow. The set-up has 127 Millions of cells and for the complete simulation, with 8192 cores approximately 3 days of computation time is needed. If the wind turbines are simulated from the start instead of introducing them in already developed turbulent flow field, it would have taken approximately 38 days of computation time with 8192 cores. As the behaviour of the wind turbine is investigated at three different heights, the procedure needs to be repeated. It will result in huge computation time requirement. With the current approach, a wind turbine simulation in urban terrain needs approximately 14 days of computation time. The limiting factor is the small time step required for the wind turbine simulations. With larger time step, other problems related to convergence and numerical stability arise. For only terrain simulation, the time step is larger than wind turbine simulation. As discussed in Sect. 2.5, current approach with overlapping grid technique and interpolation provides flexibility to introduce wind turbine in the fully developed turbulent flow field.

2.7 Evaluation

The scaled-up variant of the H-Darrieus rotor is evaluated at reference conditions **R1:AC34** of uniform inflow at 8 ms^{-1} for different tip speed ratios. After four revolutions, the forces and moments converge, and the trend shows a periodic nature.

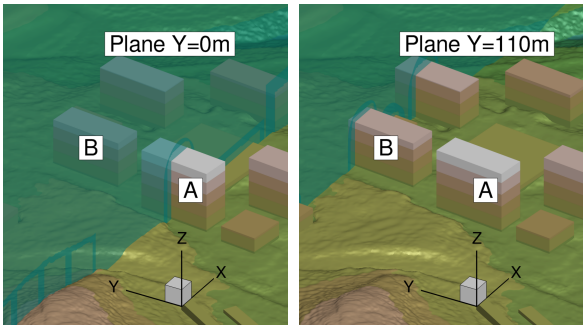

Figure 6. Post-processing planes passing through A and B.

Revolutions after this point are considered for evaluation. The moment is averaged to calculate the power coefficient for the **R1:AC35** $C_P - \lambda$ curve at reference conditions.

In urban terrain simulations, the flow field is averaged after turbulence is propagated through the complete domain. It is needed to evaluate the flow conditions at the rooftop. As shown in Fig. 6, the post-processing plane Y= 0 m passes through building A while Y= 110 m passes through building B. Based on the averaged velocity profiles and turbulence intensity, two different locations are identified at the rooftop of building A and B. At these locations, the wind turbine is placed at three distinct heights of 10 m, 12 m, and 20 m from the rooftop to investigate the influence of the skewed flow over the buildings.

For H-VAWT investigations in urban terrain, the wind turbines are simulated for a total of 42 revolutions after initialization. First 12 revolutions are not considered for the post-processing as some time is needed to develop the ~~near~~ wake of the wind turbines. The last 30 revolutions are averaged to calculate moment, tangential and normal forces along with respective standard deviations.

3 Results and discussion

The results are presented in three different subsections. First Sect. 3.1 investigates scaled H-VAWT at uniform conditions without any terrain and inflow turbulence. Second Sect. 3.2 presents the flow field analysis of the urban terrain under inflow turbulence without wind turbines. Subsequently, the behaviour of the rooftop mounted H-VAWTs in realistic conditions at different heights are discussed in Sect. 3.3.

3.1 Wind turbine simulations at uniform inflow conditions

This section compares the power coefficient, blade forces, and moment of the scaled-up wind turbine at different tip speed ratios under uniform inflow conditions with a wind speed of 8 ms^{-1}. After the near wake development, a periodic nature is observed for the variables over the revolutions. ~~The tip-speed ratios are selected from the range low $\lambda = 1.2$ to high $\lambda = 4.0$.~~ **R1:AC36** The scaled-up wind turbine is investigated at tip-speed ratios of 1.2, 1.8, 2.0, 2.75, 3.0, and 4.0. The rotational speed

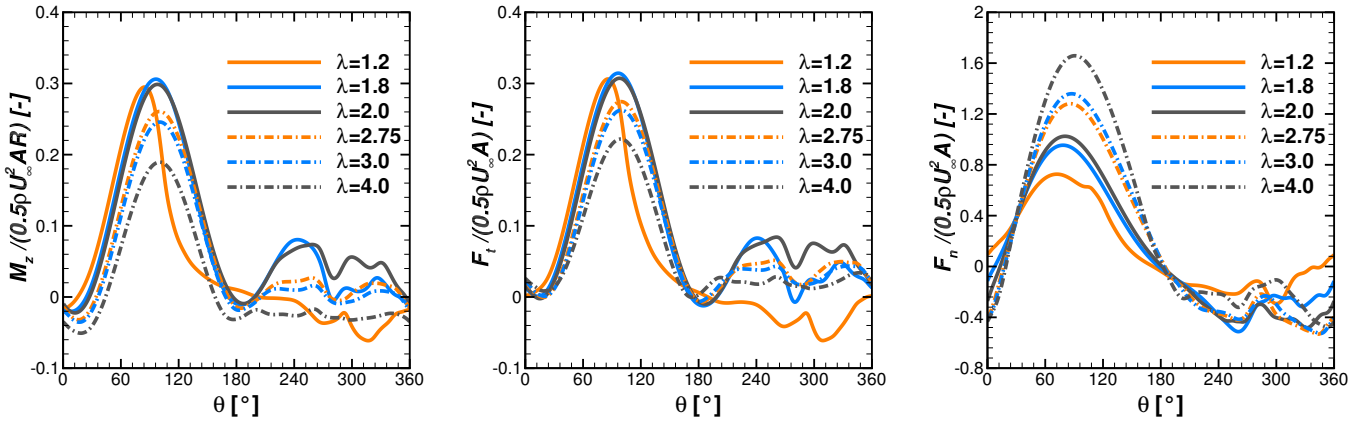

Figure 7. Normalised moment, tangential and normal forces of a single blade at different tip-speed ratio under reference conditions with uniform inflow 8 ms^{-1} without terrain.

of the wind turbine is adjusted as per ~~the~~ tip speed ratio keeping the free-stream velocity constant. **R2:Ma4** Based on chord and tangential velocity, Reynolds number Re_c ranges from 6.096×10^5 to 20.319×10^5.

Figure 7 shows the variations of normalized moment (M_Z), tangential (F_t) and normal forces (F_n) of a single blade for the different tip speed ratios during the last revolution. **R1:AC37** ~~Increasing λ results in the complex nature in moment and forces.~~ In the absence of ~~the~~ inflow turbulence, the unsteady effects on the loads and moments come from ~~the~~ phenomena like continuous change in angle of attack, blade-vortex interaction, blade wake interaction ~~involved in the operation of VAWT itself~~, **R1:AC38** which are intrinsic in the operation of VAWT. ~~The~~ **R1:AC39** A more of less sinusoidal nature can be seen in the moment curves in the first half of the revolutions for all the operating points in the left panel of Fig. 7. This part contributes most to the moment generation. In the beginning of the revolution **R1:AC40** from azimuth angles 0° to 30° ~~($0° \leq \theta° \leq 30°$)~~, an increasing λ results in lower moments. ~~Except λ =1.2~~ **R1:AC41** For all operating points from azimuth angles 75° to 180°, moment increases gradually, reaches a maximum around 90° to 100°, and then decreases gradually reaching to zero or negative at 180°. **R1:AC42** ~~Due to the rotational frame of reference, the notations for the tangential force are opposite to the moment.~~ The tangential force shown in middle panel of Fig. 7, which is responsible for the production of the moment, shows **R1:AC43** evidently an excellent correlation with the moment in left panel. **R1:AC44** ~~Except λ =1.2, with increasing tip speed ratio, the normalized tangential force also increases between $75° \leq \theta° \leq 180°$.~~ In case of λ =1.2, the moment and tangential force decreases rapidly from the maximum compared to other λ. **R1:AC45** This is attributed to the dynamic stall which is an inherent effect of the operation of a VAWT at low tip speed ratios. Similar behaviour was observed for the original unscaled H-VAWT, which has been studied by Bangga et al. (2017) for the dynamic stall phenomenon. Also, Rezaeiha et al. (2018) performed 2.5D simulations for a two-bladed H-VAWT with ~~airfoil~~ NACA0012 **R1:AC46** airfoil to investigate the influence of the operational parameters. Authors found similar behaviour at lower λ while studying the influence of the tip speed ratio on the performance. Negligible difference is observed in peak moment and tangential force for λ =1.8 and 2.0.

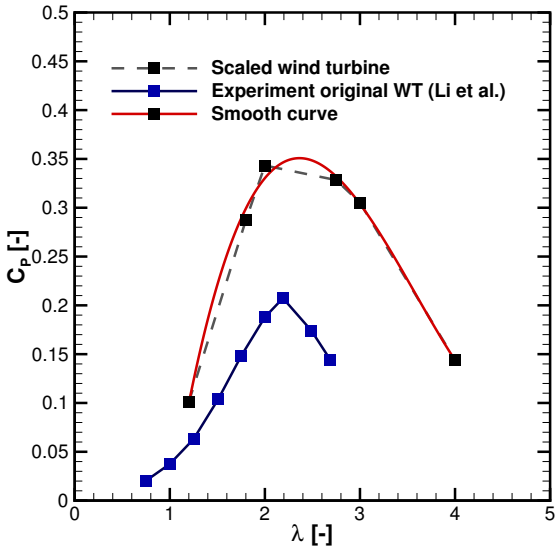

Figure 8. Power coefficient for different tip speed ratios (λ) at uniform inflow conditions. **R1:AC50**

In the second half of the revolution from azimuth angles of 180° to 360°, moments and tangential forces show a ~~not-linear~~ **R1:AC47** irregular trend. The local wind speed experienced by a blade for these azimuth positions is slowed down due to the energy extraction in the first half revolutions. **R1:AC48** ~~, which leads to the stalled conditions.~~ Fluctuations are observed in moment and tangential force at azimuth position from 240° to 330°, as blade wake interaction has dominant effect in second half revolution. The influence of the shaft can be seen as a sudden drop in tangential force and jump in normal force at 270° azimuth position. For λ =1.8 and 2.0, the wind turbine generate relatively higher moment in the second half revolution compared to other tip speed ratios. However, the magnitude is far lower than the first half of the revolution. With increasing λ, the nature of the curve flattens in the second half of the revolutions **R1:AC49** implying very small moment generation and decrease in the influence of the wake caused by the shaft. At higher λ, an increase in rotational speed results in larger effective blockage to the flow. It creates large deficit in the streamwise velocity in wake, which also affects the wake generated from shaft.

The right panel of Fig. 7 shows variations in normal forces. As the blade moves further from azimuth 0°, the normal force ~~decreases~~ **R1:AC42** increases, gradually reaching to a **R1:AC42** maximum ~~minimum~~ around azimuth 100-105° and then ~~increases~~ **R1:AC42** it decreases. After 180° azimuth position, the direction of the force is reverted. Unlike the moment and tangential force, the normal force increases for λ >1.8. The effect of shaft can be seen at azimuth position of 270°.

The ~~coefficients of~~ power coefficient of scaled-up version at different operating points along with smooth curve and experimental values for original wind turbine (Li et al. (2016)) are shown in Fig. 8. **R1:AC50** The scaled-up wind turbine shows improvement in the power coefficient at all considered tip speed ratios. By scaling up, the Reynolds number based on chord increases, which

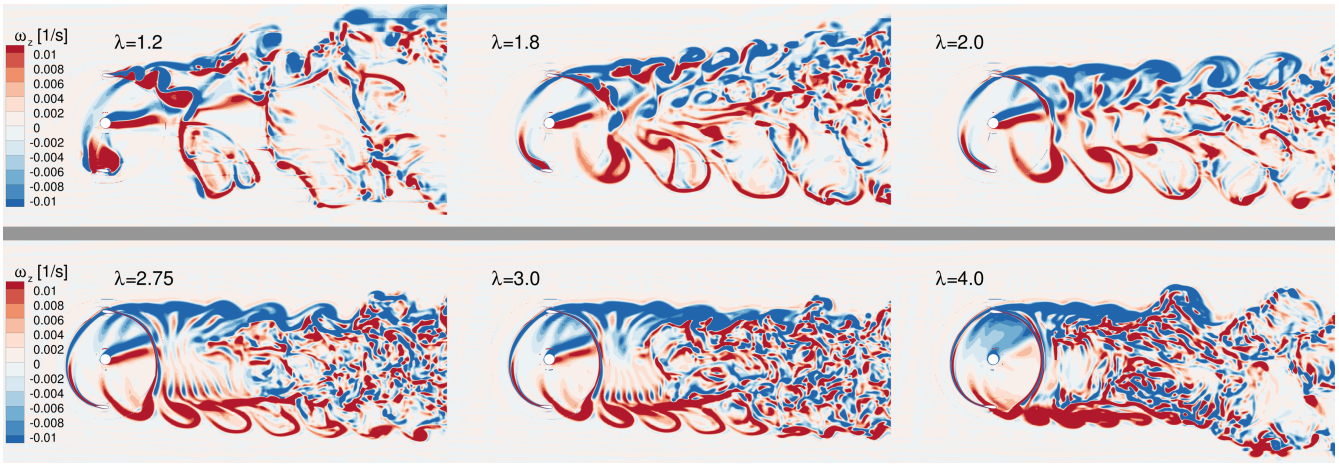

Figure 9. **R2:Ma2b** Z vorticity contour at different tip speed ratio.

results in enhancement of the power of the H-VAWT. Roh et al. (2013) studied effect of Reynolds number on the straight bladed VAWT. The study found that the power production of the VAWT is directly dependent on the Reynolds number. Rezaeiha et al. (2018) studied impact of operational parameters on characteristic of VAWT and concluded that increasing chord based Reynolds number Re_c significantly improves the turbine performance. For the scaled up wind turbine, C_p increases with λ, reaching to a maximum of 0.35 for $2 < \lambda < 2.75$, and then decreases. ~~The power coefficient differs despite having a similar trend for λ =1.8 and 2.0 in normalized moment shown in the left panel of the Fig. 7.~~ **R1:AC51** The normalized moment curves for $\lambda = 1.8$ and 2.0 are almost identical as depicted in the left panel of the Fig. 7. However, the larger rotational speed for $\lambda = 2$ results into higher C_P. ~~On the contrary, the normalized moment for $\lambda = 2$ and 2.75 varies considerably, but C_p differs by a small margin. These differences are be attributed mainly to the changes in rotational speed and subsequently to the operating point.~~ **R1:AC52** Similarly, the normalized moment for $\lambda = 2$ and 2.75 varies considerably, but C_P differs by a small amount. For λ larger than λ_{opt}, the thrust increases while power decreases. It results in decreasing C_P. As $\lambda = 2.75$ is near to λ_{opt}, it is selected for the wind turbine investigation in urban terrain. Details are discussed in Sect. 3.3.

R2:Ma2b In Fig. 9, Z vorticity contours in the horizontal plane passing though the rotor have been depicted for different tip speed ratios. There are significant differences in the wakes of low, middle and high tip speed ratios. Particularly, it can be seen, how vortices are formed and how they propagate into the wake. For λ =1.2, no coherent vortical structures can be seen in wake. In case of λ =1.8 and 2.0, the coherent vortical structures are dominant in the wake and they propagate over long distance in downstream. Further increase in λ results in early break down of vortical structures in downstream of the rotor. It can be clearly seen in case of $\lambda = 3.0$ and 4.0. The temporal frequency of the vortex shedding relative to the freestream increases with increase in tip speed ratio. It leads to the stacking of the shed vortices and shear layers in the wake as well as behind the upwind passage of blades. Therefore, the wake profile is strongly dependent on the tip speed ratio.

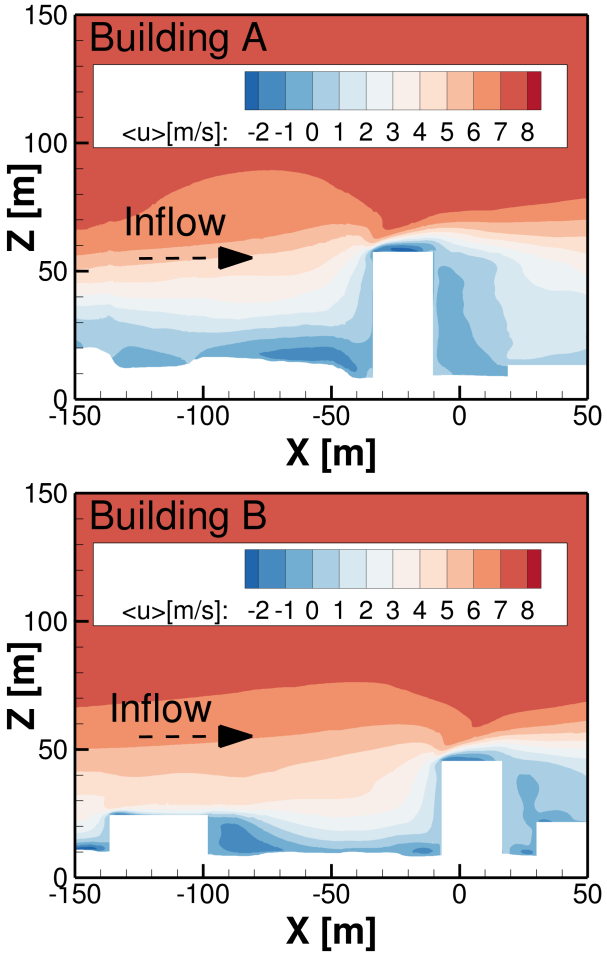

Figure 10. R2:Ma5 R1:AC54 Distribution of averaged u component of velocity in the Plane Y = 0 m and Y = 110 m passing through building A and B.

3.2 Urban terrain simulations under turbulent inflow

This section analyzes the flow field in the urban terrain under application of a log law wind profile and inflow turbulence in absence of wind turbines. **R1:AC53** ~~However,~~ The results from these studies is the basis for the wind turbine investigations in turbulent urban conditions, which are discussed in Sect. 3.3.

The averaged flow variables are analyzed in two different planes along the flow direction at the rooftops of the buildings A and B. The plane Y=0 m passes through approximately the middle of the A while plane Y=110 m passes through the left part of the B relative to the flow direction, as shown in Fig. 6. The flow field is averaged for approximately four minutes after the

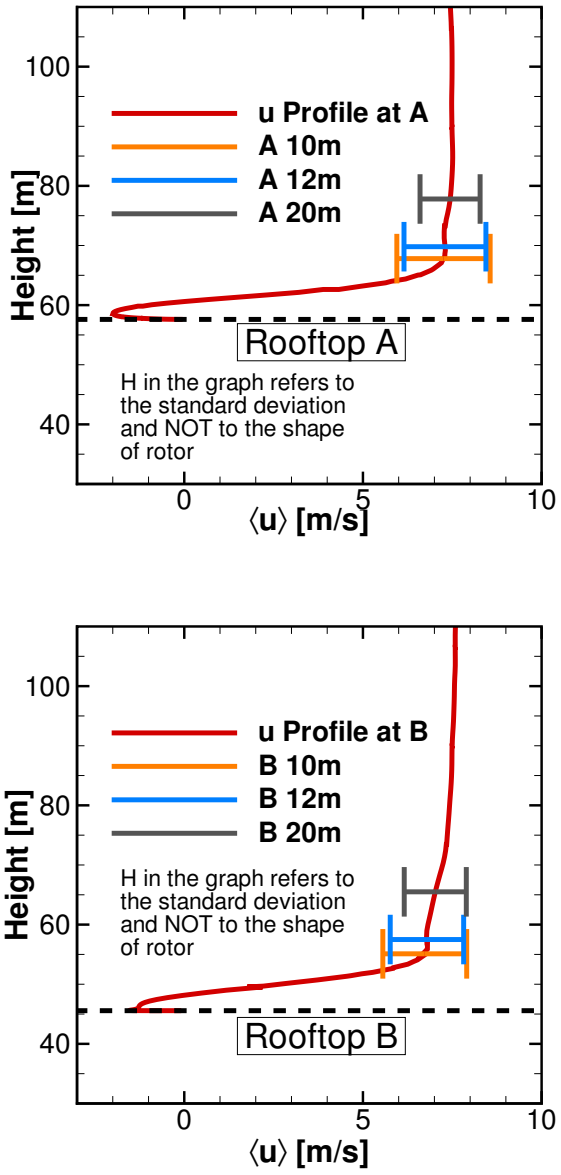

Figure 11. Mean velocity Profile and standard deviations at positions above rooftops of A and B. **R1:AC55**

turbulence is fully developed and is propagated through the domain. Figure 10 shows the distribution of the averaged flow field at building A and building B. Based on the accelerated velocity region, the location for the wind turbines are selected as X= -27 m and X= 0 m at the rooftops of A and B, respectively. For the wind turbine investigations later on, 10 m, 12 m, and 20 m heights from the rooftop to the center of the blade heights are chosen, as discussed in Sect. 2.5.

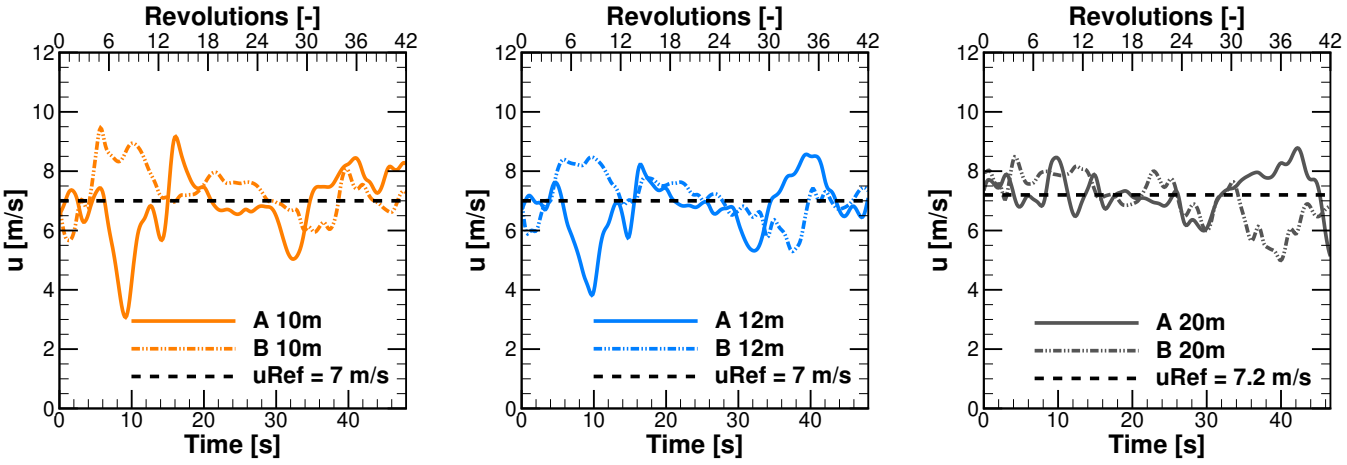

Figure 12. Time series of u component of velocities at different rooftop heights above building A and B.

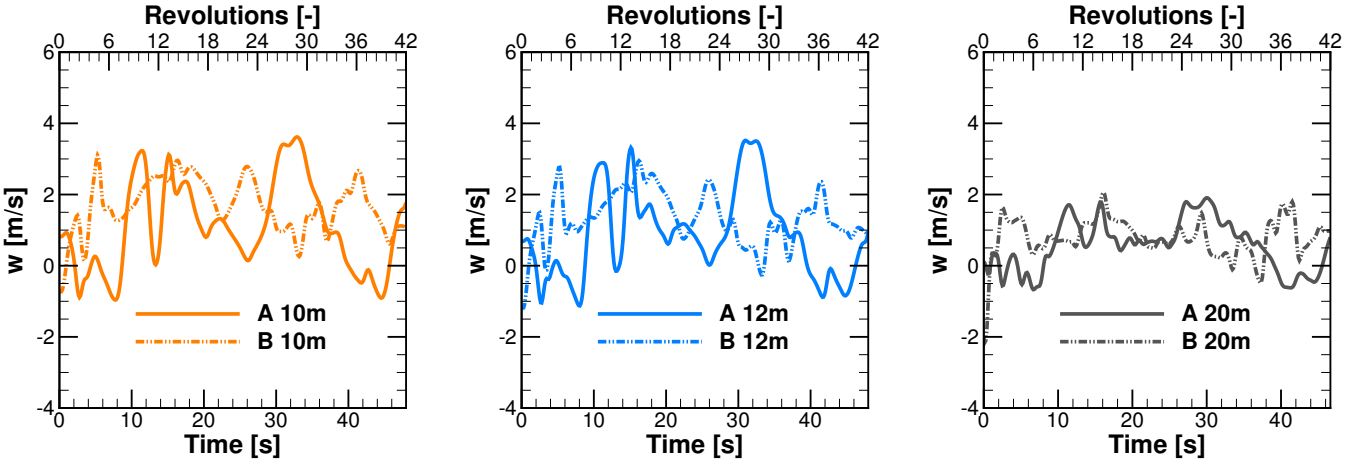

Figure 13. Time series of w component of velocities at different rooftop heights above building A and B. **R1:AC58**

The mean velocity profiles and standard deviations at the selected positions over the rooftop of A and B are shown in Fig. 11. At the 10 m and 12 m heights, the standard deviations are higher than 20 m height, which is evident as these positions are close to the rooftop. Along with the upstream turbulence originating from vegetation and topography, the separation caused due to the leading edges influences the nearby rooftop region. **R1:AC55** The mean wind velocity (u and w components), turbulence intensity, skew angle and standard deviation at different heights from the rooftop are given in Table 3. With increasing distance from the rooftop, the magnitude of mean wind speed increases slightly while drop in turbulence intensity is observed. The near rooftop positions are expected to experience higher skew angles than at 20 m height. The maximum skew angle of approx.

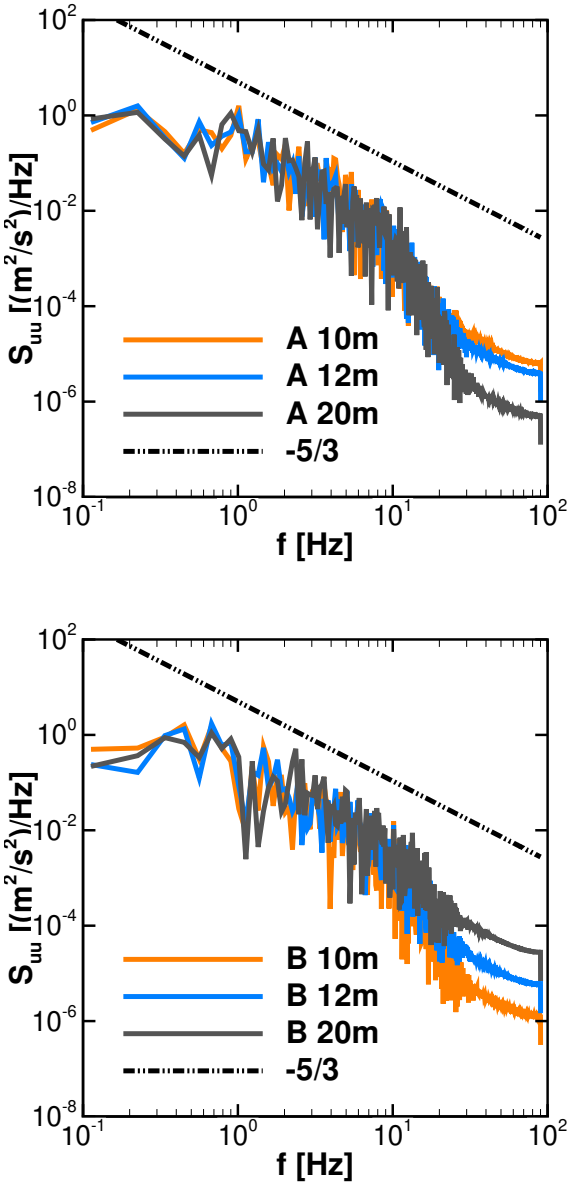

Figure 14. Power spectral density S_{uu} of u component of the velocity at wind turbine positions.

355 12.5° occurs at the height of 10 m over the rooftop of A. The flow over rooftop of A appears to be more skewed than over rooftop of B.

For the wind turbine positions above the rooftops of A and B, time series of u and **R1:AC58** w component of velocity are shown in Fig. 12 and **R1:AC58** in Fig. 13, respectively. The wind turbines are simulated for these time series. The vertical component over different positions vary significantly over range from -2 ms^{-1} to 4 ms^{-1} with mean value being

Table 3. Mean wind speeds and turbulence intensities at the rooftop. **R1:AC56, 1:AC57, 1:AC59**

Case name	mean u (ms^{-1})	mean w (ms^{-1})	Skewness $\beta(°)$	Turbulence intensity (%)	σ_u (ms^{-1})
A 10 m	7.26	1.58	12.32	15.24	1.30
A 12 m	7.29	1.41	10.93	13.82	1.15
A 20 m	7.45	0.88	6.74	9.52	0.84
B 10 m	6.77	1.56	6.68	13.94	1.17
B 12 m	6.78	1.34	6.41	12.99	1.03
B 20 m	7.02	0.83	5.26	10.65	0.87

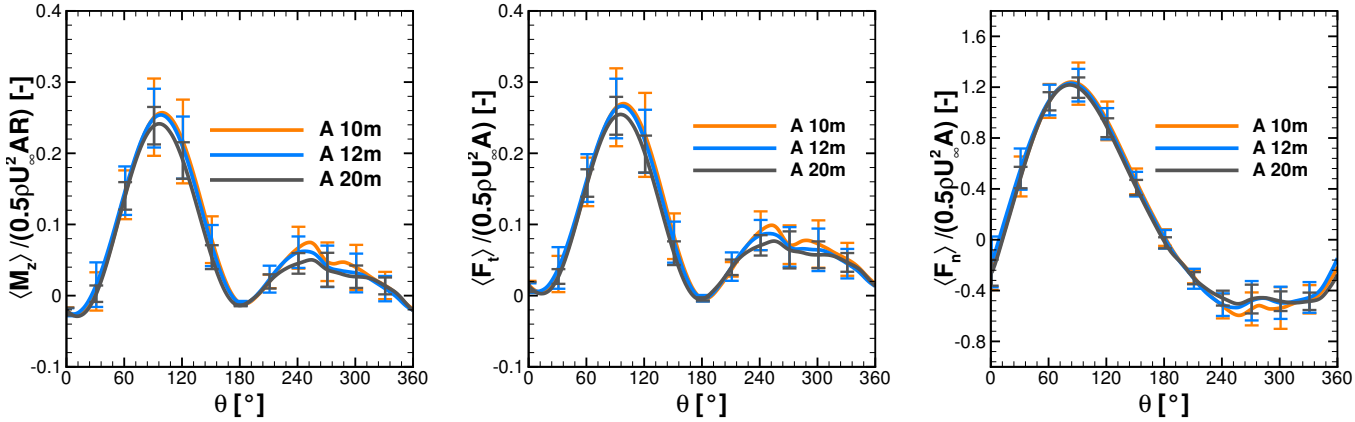

Figure 15. Normalised moment, tangential and normal forces of a single blade at $\lambda = 2.75$ under turbulent inflow at rooftop of A. **R1:AC63**

positive. It results in skewed flow over rooftop. The power spectral density S_{uu} for the u component for different positions is shown in Fig. 14. The curves at all turbine positions show good agreement in the region of the inertial range of scales with the Kolmogorov $f^{-5/3}$ spectrum. It indicates that the turbulence is propagated effectively through the domain till the relevant positions of the wind turbines.

3.3 Wind turbines simulations in urban terrain

This section presents the analysis of the wind turbines at different heights above the rooftops of A and B. As discussed in Sect. 2.5, the wind turbines are initialized in the developed turbulent flow field and simulated further. The objective of

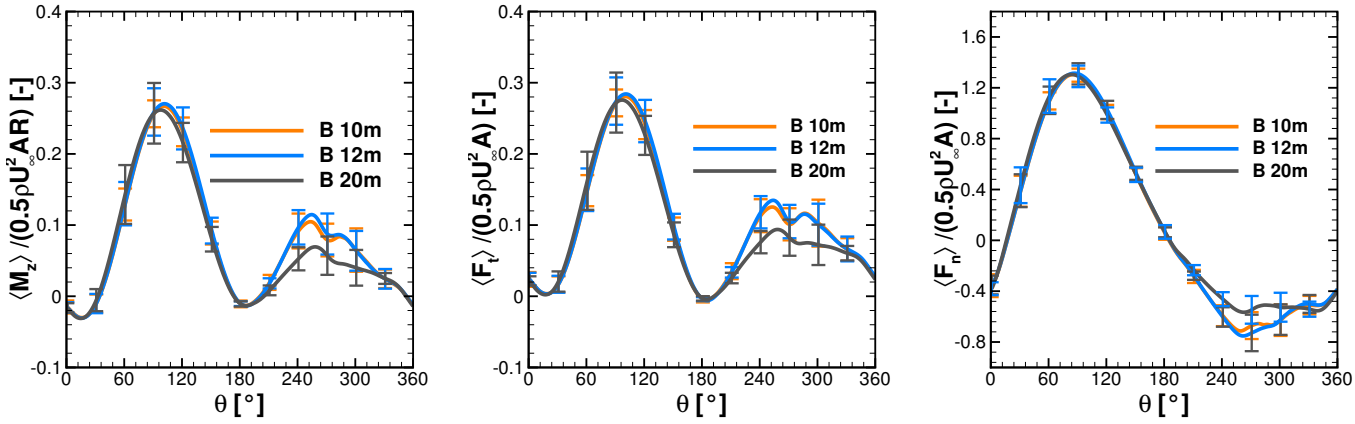

Figure 16. Normalised moment, tangential and normal forces of a single blade at $\lambda = 2.75$ under turbulent inflow at rooftop of B.

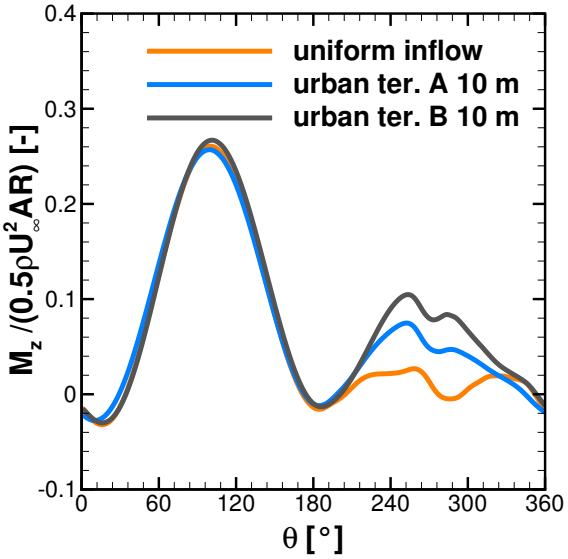

Figure 17. Normalized moment of a single blade in uniform inflow and in urban terrain at 10 m height from rooftop of A. (Note: In case of urban terrain, moment is first averaged before normalized.) **R1:AC66**

these simulations is to investigate the behaviour of the H-Darrieus wind turbine under the turbulent inflow influenced by the vegetation and the topography of the urban terrain.

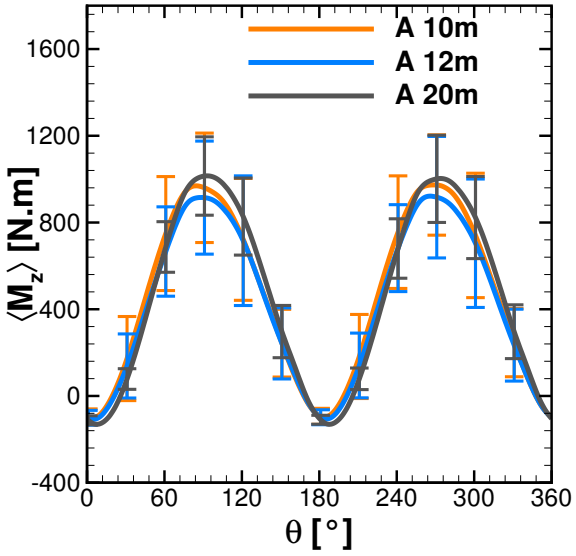

Figure 18. Moment of the complete Rotor at different heights over rooftop of A. **R1:AC67**

At the considered heights, **R1:AC60** ~~long~~ averaged wind speeds vary slightly from each other in the range $\pm 0.5\ \mathrm{ms}^{-1}$, as shown in Table 3. Also, from Fig. 12, instantaneous velocities fluctuates roughly around the respective mean values except for some large deviations in considered time series for wind turbine investigations.Therefore, it was assumed that the wind turbines positioned at 10 m, 12 m heights above rooftops of A and B operate at a mean wind speed of $7\ \mathrm{ms}^{-1}$ and at 20 m heights, they operate at a mean wind speed of $7.2\ \mathrm{ms}^{-1}$. Later, these same mean values of velocity are used for the normalization of the forces and the moments. ~~Subsequently, the rotational speeds are deduced depending on the wind speed and the operating point of λ =2.75. The selected tip speed ratio λ = 2.75 lies near to the optimum λ.~~ **R1:AC61a** These mean wind velocities are reasonably close to $8\ \mathrm{ms}^{-1}$, at which reference cases are simulated. From Fig. 8, the $\lambda = 2.75$ is near to the optimum λ. Subsequently, for the investigations of H-VAWT in urban terrain, the rotational speeds are deduced depending on the selected wind speed and the operating point of λ =2.75. ~~The variables are averaged after 12 revolutions so that the near wake flow field of the wind turbine is well developed. The variables are recorded for total of 42 revolutions. However, last 30 revolutions are considered for the analysis.~~ **R1:AC62** The instantaneous variables like moments, tangential and normal forces are recorded for total of 42 revolutions under turbulent inflow. However, only the last 30 revolutions are averaged later in post processing and considered for the analysis. Initial 12 revolutions are ignored so that the flow field near wind turbine and wake are well developed.

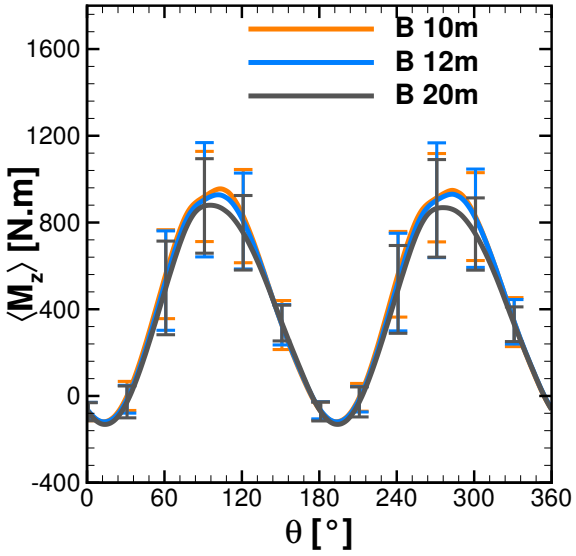

Figure 19. Moment of the complete rotor at different heights over rooftop of B. **R1:AC67**

Figure 15 and Fig. 16 show the phase averaged and normalized moment, tangential, and normal forces of a single blade and standard deviation at different heights over the rooftop of A and B. As shown in the left panel in Fig. 15, the averaged moments show an identical characteristic over the first half revolution of wind turbine at 10 m, 12 m, and 20 m height above the rooftop of building A. However, the standard deviation contours indicate **R1:AC64** that the moment deviates significantly between azimuth positions from 60° to 120° and 240° to 300°. The normalized moment from Fig. 15 is compared with the uniform inflow case at $\lambda = 2.75$ from Fig. 7. **R1:AC65** It can be seen that at all considered heights the normalized moment has been increased in the second half revolutions implying the better performance, particularly at azimuth positions between 200° to 270°. **R1:AC66**, **R1:AC68** The left panel of Fig. 16 also reveals a consistent trend for a normalized moment over the second half revolution. The normalized moments of single blade at 10 m height over A and B are compared with reference case in Fig. 17 in order to visualize better performance in the second half revolutions. This improvement is attributed to the combined effect of turbulence and skewness of flow near rooftop. Due to the skewed flow over rooftop, the bottom part of the blade in the downwind section is less impacted by the wake generated by upwind passage of the other blade. Therefore, the reduced blade wake interaction in downwind section improves the performance by generating positive moment. These findings are also in line with the study of Mertens et al. (2003), which concluded that the performance coefficient of a H-Darrieus wind turbine in skewed flow, based on the projected frontal rotor area, can increase above that of non-skewed flow. Orlandi et al. (2015) investigated H-rotor with 3D URANS approach in skewed flow and reported a similar phenomenon in moment and forces.

Table 4. Power coefficients of wind turbine at different heights over A and B. **R1:AC67**

Height over rooftop [m]	Power coefficient C_p over A	Power coefficient C_p over B
10 m	0.415	0.385
12 m	0.385	0.374
20 m	0.393	0.332

Middle panels of Fig. 15 and Fig. 16 represent normalized tangential force at different heights over rooftop of A and B. It shows excellent correlation with normalized moments. Showing excellent correlation to the moment, the high standard deviations are seen in the first half revolutions, including at peak position around 90-95° implying the influence by the complex inflow conditions. Also, similar trend can be seen over second half revolutions. **R1:AC70** The higher magnitude of the standard deviation indicates that due to turbulence, flow conditions in the downstream part are more random, which result in "less phase locked" trend in the forces. The right panel from Fig. 15 and Fig. 16 show the normalized normal forces experienced by a single blade at different heights above the rooftop of A and B. The lower magnitudes of standard deviations and overlapping curves for the different heights for the first half revolutions indicate that normal forces are less sensitive to turbulence and skewed inflow. However, in second half revolutions relatively higher values of standard deviations can be seen.

The phase averaged moment over 30 revolutions for complete rotor is shown in Fig. 18 and Fig. 19 for different heights over the rooftop of A and B, respectively. **R1:AC72** The higher standard deviations in the moment of the complete rotor over different azimuth positions indicate the influence of complex turbulence inflow conditions on wind turbine performance. ~~The moment plots of the complete rotor and standard deviation indicate that the complex inflow conditions significantly impact wind turbine performance.~~ For the peak position around 90° to 95° and 270° to 275°, it can be observed that the upper and lower limits **R1:AC73** of the moment lie in the range of approx. $\pm 20 - 25\%$. At the azimuth positions of 0° $\pm 30°$ and $180° \pm 30°$, the standard deviation is small. The power coefficient for the considered heights are given in Table 4. The near rooftop heights show increase in power coefficient compared to uniform inflow case, where the power coefficient for λ =2.75 is 0.33. **R1:AC74** ~~The coefficients of power are given in the second plot of Fig. 18 and 19~~. As the power extracted by the wind turbine is directly proportional to the power of wind speed, the overall sum of a positive and negative deviations in the wind speed leads to a positive increase in power. It can be illustrated by a simple mathematical expression as $(a+b)^3 - a^3 > a^3 - (a-b)^3$. It translates that even if the mean wind speed is the same, the higher turbulence case will contain more energy **R1:AC75** (Putnam, 1948)(Möllerström et al., 2016). In the present study, even though the averaged wind speeds at all considered heights are lower than the uniform inflow case, the coefficients of power are still higher than that of the uniform case of $\lambda = 2.75$ shown in Fig. 8. Turbulence and the skewed flow, both contribute positively enhancing performance. **R1:AC76** ~~Figure ?? shows the resolved wake of H-VAWT in turbulent inflow at a height of 10m above building B.~~

4 Conclusions

In the present study, a numerical investigation of the influence of the complex and urban terrain on the behaviour of the rooftop mounted vertical axis wind turbine (H-VAWT) under turbulent inflow conditions are performed. The high-fidelity scale resolving DDES simulation and higher order numerical scheme are employed to investigate the in-stationary characteristics of the forces and moment of the vertical axis wind turbine.

In first part of study, the behaviour of the scaled-up, two straight ~~balded~~ **R1:AC77** bladed H-VAWT with NACA0021 airfoil section is investigated at uniform inflow of 8 ms^{-1} over different tip speed ratios. The scaled-up wind turbine has a diameter of 7 m, blade length of 4.2 m, and a fixed pitch angle of 6°. It is found that the wind turbine shows better performance than original design due to increase in the chord based Reynolds number by scaling up. Based on the tip speed ratio vs. power coefficient curve ($C_P - \lambda$), an operating point $\lambda = 2.75$ is selected for investigation of H-VAWT in urban terrain, as it is near to optimum λ. In the second part of study, the flow field in the realistic terrain consisting of different buildings, vegetation, and topographical features under turbulent inflow is investigated. The flow variables are averaged after turbulence is well developed and propagated through the computational domain. The mean wind profiles, turbulence levels and flow skewness are analysed above the rooftops of two distinct buildings. Based on the mean wind velocities and selected operating point $\lambda = 2.75$, the rotational speed is derived for H-VAWT investigation in urban terrain.

The last part of study, H-VAWT is investigated at different heights over rooftop of buildings. The wind turbine meshes are introduced in instantaneous flow field from second part by application of overlapping grid technique and interpolation. By this simulation strategy, wind turbines are investigated in a turbulent flow field with convenience and a significant reduction in the computation cost. **R1:AC80** Based on the averaged forces and moments over multiples revolutions, the H-VAWT shows significant improvement in the performance at heights of 10 m and 12 m from the rooftop of buildings in considered realistic urban terrain. At these heights, it operates in the flow with a relatively higher level of turbulence and skewed angle than the 20 m height. Due to the skewed flow, the reduced blade wake interaction in the second half revolutions (downwind) increases tangential forces and moment extraction compared to the uniform non-skewed flow case. Large deviations are observed in the tangential forces and moments due to temporal changes. The improvement in the performance at near rooftop heights is due to the combined influence of the turbulence and skewed angle of the flow. Also, the H-VAWT placed at the height of 20 m from rooftops shows a better power coefficient than the uniform inflow conditions. **R1:Ma2** Therefore, it can be concluded that combined turbulence and skewness, has a positive impact on performance of rooftop mounted H-VAWT in considered urban terrain and turbulence inflow data, when operated at fixed tip speed ratio.

Author contributions. PZ conducted the CFD investigations and wrote the paper. TL initiated the research, supervised the work and revised the manuscript.

Competing interests. Authors declare that they have no conflict of interest.

Acknowledgements. Authors gratefully acknowledge the High Performance Computing Center Stuttgart for providing computational resources within the project WEALoads. The studies are conducted for the project "Loads and performance of the small wind turbine in urban environment" under "Joint Graduate Research Training Group Windy Cities", which is funded by Ministry of Science, research and arts, Baden Württemberg. Also, authors acknowledge Amgad Dessoky for providing the original computation grids of the wind turbine from the validation study.

References

Balduzzi, F., Bianchini, A., Carnevale,E.A, Ferrari L., and Magnani, S.: Feasibility analysis of a Darrieus vertical-axis wind turbine installation in the rooftop of a building, Applied Energy, 97, 921-929, https://doi.org/10.1016/j.apenergy.2011.12.008., 2011

Mithraratne, N.: Roof-top wind turbines for microgeneration in urban houses in New Zealand, Energy and Buildings, 41, Issue 10, 1013-1018, https://doi.org/10.1016/j.enbuild.2009.05.003., 2009

van Wijk, B. M.:Predicting the rooftop wind climate for urban wind energy in the Rotterdam - Delft - Zoetermeer region: new approaches for implementing urban height data in the wind atlas method, Master Thesis, TU Eindhoven/TU Delft,Netherlands, 136 pp., 2011

Toja-Silva, F., Colmenar-Santos, A., and Castro-Gil, M.: Urban wind energy exploitation systems: Behaviour under multidirectional flow conditions—Opportunities and challenges, Renewable and Sustainable Energy Reviews, 24, 364-378, https://doi.org/10.1016/j.rser.2013.03.052. 2013

KC, A., Whale, J., and Urmee, T.: Urban wind conditions and small wind turbines in the built environment: A review, Renewable Energy, 131, 268-283, 0960-1481, https://doi.org/10.1016/j.renene.2018.07.050., 2019

Karadag, I., and Yuksek, I. : Wind Turbine Integration to Tall Buildings, Renewable Energy - Resources, Challenges and Applications, IntechOpen, DOI: 10.5772/intechopen.91650, 2020

Bianchi, S., Bianchini, A., Ferrara, G., and Ferrari, L. : Small Wind Turbines in the Built Environment: Influence of Flow Inclination on the Potential Energy Yield. Proceedings of the ASME Turbo Expo 2013: Turbine Technical Conference and Exposition. Volume 8, https://doi.org/10.1115/GT2013-95637, 2013

Mertens, S., van Kuik, G., and van Bussel, G.: Performance of an H-Darrieus in the Skewed Flow on a Roof." ASME. J. Sol. Energy Eng. November 2003; 125(4): 433–440. https://doi.org/10.1115/1.1629309

Möllerström, E., Ottermo, F., Goude, A., Eriksson, S., Hylander, J., and Bernhoff H.:Turbulence influence on wind energy extraction for a medium size vertical axis wind turbine, Wind Energ. 2016; 19:1963–1973, DOI: 10.1002/we.1962, 2016

Bertényi, T., Wickins, C., and McIntosh, S.: Enhanced Energy Capture Through Gust-Tracking in the Urban Wind Environment, 48th AIAA Aerospace Sciences Meeting Including the New Horizons Forum and Aerospace Exposition, Doi:10.2514/6.2010-1376, 2016

Pagnini, L.c., Burlando, M.,and Repetto, M.P. : Experimental power curve of small-size wind turbines in turbulent urban environment, Applied Energy, Volume 154, 112-121, Doi: https://doi.org/10.1016/j.apenergy.2015.04.117., 2015

Kooiman, S., and Tullis, S.: Response of a Vertical Axis Wind Turbine to Time Varying Wind Conditions Found within the Urban Environment. Wind Engineering. 34. 10.1260/0309-524X.34.4.389, 2010

Trivellato, F., and Castelli, M. R.: On the Courant–Friedrichs–Lewy criterion of rotating grids in 2D vertical-axis wind turbine analysis, Renewable Energy, 62, 53-62, Doi https://doi.org/10.1016/j.renene.2013.06.022., 2014

Balduzzi, F., Zini, M., Molina, A.C., Bartoli, G., De Troyer, T., Runacres, M.C., Ferrara, G., Bianchini, A. Understanding the Aerodynamic Behavior and Energy Conversion Capability of Small Darrieus Vertical Axis Wind Turbines in Turbulent Flows. Energies 2020, Volume 13, Page 2936. https://doi.org/10.3390/en13112936

Lam, H.F., and Peng, H.Y. : Study of wake characteristics of a vertical axis wind turbine by two- and three-dimensional computational fluid dynamics simulations, Renewable Energy, Volume 90, Pages 386-398, https://doi.org/10.1016/j.renene.2016.01.011., 2016

Dessoky, A., Lutz, T., Bangga, G., and Krämer, E., Computational studies on Darrieus VAWT noise mechanisms employing a high order DDES model, Renewable Energy, Volume 143, Pages 404-425, https://doi.org/10.1016/j.renene.2019.04.133 , 2019

Patil, R.; Daróczy, L.; Janiga, G.; Thévenin, D.: Large eddy simulation of an H-Darrieus rotor. Energy 2018, 160, 388–398.

Brahimi, M. T., and Paraschivoiu, I. (May 1, 1995). "Darrieus Rotor Aerodynamics in Turbulent Wind." ASME. J. Sol. Energy Eng. May 1995; 117(2): 128–136. https://doi.org/10.1115/1.2870839

M. Salman Siddiqui, Adil Rasheed, Trond Kvamsdal, Mandar Tabib, Effect of Turbulence Intensity on the Performance of an Offshore Vertical Axis Wind Turbine, Energy Procedia, Volume 80, 2015, Pages 312-320, ISSN 1876-6102, https://doi.org/10.1016/j.egypro.2015.11.435.

Abdolrahim Rezaeiha, Hamid Montazeri, Bert Blocken, Characterization of aerodynamic performance of vertical axis wind turbines: Impact of operational parameters, Energy Conversion and Management, Volume 169, 2018, Pages 45-77, ISSN 0196-8904, https://doi.org/10.1016/j.enconman.2018.05.042.

M. Salman Siddiqui, Muhammad Hamza Khalid, Rizwan Zahoor, Fahad Sarfraz Butt, Muhammed Saeed, Abdul Waheed Badar, A numerical investigation to analyze effect of turbulence and ground clearance on the performance of a roof top vertical–axis wind turbine, Renewable Energy, Volume 164, 2021, Pages 978-989, ISSN 0960-1481, https://doi.org/10.1016/j.renene.2020.10.022.

A. Orlandi, M. Collu, S. Zanforlin, A. Shires, 3D URANS analysis of a vertical axis wind turbine in skewed flows, Journal of Wind Engineering and Industrial Aerodynamics, Volume 147, 2015, Pages 77-84, https://doi.org/10.1016/j.jweia.2015.09.010.

Q. Li, T. Maeda, Y. Kamada, J. Murata, M. Yamamoto, T. Ogasawara, K. Shimizu, T. Kogaki, Study on power performance for straight-bladed vertical axis wind turbine by field and wind tunnel test, Renewable Energy, Volume 90, 2016, Pages 291-300, https://doi.org/10.1016/j.renene.2016.01.002.

P. Letzgus, T. Lutz, E. Krämer Detached Eddy Simulations of the local Atmospheric Flow Field within a Forested Wind Energy Test Site located in Complex Terrain, Journal of Physics: Conference Series, Volume 1037, 2018, Pages 072043, https://doi.org/10.1088/1742-6596/1037/7/072043.

R.H.Shaw, U. Schumann Large-eddy simulation of turbulent flow above and within a forest, Boundary-Layer Meteorology, Volume 61, 1992, Pages 47-64, https://doi.org/10.1007/BF02033994.

J. Mann Wind field simulation, Probabilistic Engineering Mechanics, Volume 13, 1998, Pages 269-282, https://doi.org/10.1016/S0266-8920(97)00036-2

N. Troldborg, J. N. Sørensen, R. Mikkelsen, N. N. Sørensen A simple atmospheric boundary layer model applied to large eddy simulations of wind turbine wakes, Wind Energy, Volume 17, 2014, Pages 657-669, https://doi.org/10.1002/we.1608

C. Rossow, N. Kroll, D. Schwamborn The MEGAFLOW Project – Numerical Flow Simulation for Aircraft, Progress in Industrial Mathematics at ECMI 2004, 2006, Pages 3-33

J. Benek, P. Buning, J. Steger A 3-D chimera grid embedding technique, 7th Computational Physics Conference, 1985, https://doi.org/10.2514/6.1985-1523

U. Schäferlein, C. Oehrle, M. Hollands, M. Keßler, E. Krämer, Computation of Helicopter Phenomena Using a Higher Order Method, 2013, Pages 423-438, https://doi.org/10.1007/978-3-319-02165-2_29

P. Weihing, J. Letzgus, G. Bangga, T. Lutz, E. Krämer, Hybrid RANS/LES Capabilities of the Flow Solver FLOWer—Application to Flow Around Wind Turbines, Progress in Hybrid RANS-LES Modelling, 2018, Pages 369-380, https://doi.org/10.1007/978-3-319-70031-1_31

R. F. Menter, Two-equation eddy-viscosity turbulence models for engineering applications, AIAA Journal, volume = 32, 1994, Pages 1598-1605, https://doi.org/10.2514/3.12149

A. Jameson, W. Schmidt, E. Turkel, Numerical solution of the Euler equations by finite volume methods using Runge Kutta time stepping schemes, 14th Fluid and Plasma Dynamics Conference, 1981, volume = 32, https://arc.aiaa.org/doi/abs/10.2514/6.1981-1259

R. Bravo, S. Tullis, S. Ziada, S., Performance Testing of a Small Vertical-Axis Wind Turbine, Proceedings of the 21st Canadian Congress of Applied Mechanics (CANCAM07), 2007

I. Baring-Gould, J. Fields, F. Oteri, R. Preus, Deployment of Wind Turbines in the Built Environment: Risks, Lessons, and Recommended Practices, 2017, https://www.osti.gov/biblio/1361457

C. J. Ferreira, H. Bijl, G. van Bussel, G. van Kuik, Simulating Dynamic Stall in a 2D VAWT: Modeling strategy, verification and validation with Particle Image Velocimetry data, 2007, Volume = 75, Pages 012023, Journal of Physics: Conference Series, https://doi.org/10.1088/1742-6596/75/1/012023

G. Bangga, T. Lutz, A. Dessoky, E. Krämer Unsteady Navier-Stokes studies on loads, wake, and dynamic stall characteristics of a two-bladed vertical axis wind turbine, 2017, Volume 9, pages 053303, Journal of Renewable and Sustainable Energy, https://doi.org/10.1063/1.5003772

L. Kern, J.V. Seebaß, J. Schlüter, Das Potenzial von vertikalen Windenergieanlagen im Kontext wachsender Flächennutzungskonflikte und Akzeptanzprobleme der Windenergie, 2019, Volume 43, pages 289-302, Zeitschrift für Energiewirtschaft, https://doi.org/10.1007/s12398-019-00264-7

R. Gasch, and J. Twele, Wind power plants: Fundamentals, design, construction and operation, second edition, 2012, https://doi.org/10.1007/978-3-642-22938-1

A. Tosatto, S. Chatzivasileiadis, HVDC loss factors in the Nordic power market, Electric Power Systems Research, Volume 190, 2021, 106710, ISSN 0378-7796, https://doi.org/10.1016/j.epsr.2020.106710

M. Kinzel, Q. Mulligan and J. O. Dabiri, Energy exchange in an array of vertical-axis wind turbines, Journal of Turbulence, 13:, 2012, https://doi.org/10.1080/14685248.2012.712698

J. O. Dabiri , Potential order-of-magnitude enhancement of wind farm power density via counter-rotating vertical-axis wind turbine arrays, Journal of Renewable and Sustainable Energy 3, 04310, 2011, https://doi.org/10.1063/1.3608170

P. C. Putnam, Power from the wind, Van Nostrand Reinhold Company, NY, 1948

S.-C. Roh, and S.-H. Kang, Effects of a blade profile, the Reynolds number, and the solidity on the performance of a straight bladed vertical axis wind turbine, Journal of Mechanical Science and Technology, 2013, Volume 27, Pages 3299–3307 https://doi:10.1007/s12206-013-0852-x

T. C. Hohman, L. Martinelli, and A. J., The effects of inflow conditions on vertical axis wind turbine wake structure and performance, Journal of Wind Engineering and Industrial Aerodynamics, Volume 183, Pages 1–18 https://doi:10.1016/j.jweia.2018.10.002